Materials Research. 2024; 27:e20230495
DOI: https://doi.org/10.1590/1980-5373-MR-2023-0495

Investigation of Wear Behavior in Ni-Ti-SiC Composites Fabricated via Microwave Sintering

P. Hariprasad[a]*, K.Kumaresan[b], Bader Alqahtani[c], Abdulkarim Alansari[c]

[a]*KIT-Kalaignar Karunanidhi Institute of Technology, Department of Mechanical Engineering, Coimbatore, India.*
[b]*Park College of Engineering and Technology Department of Mechanical Engineering, Coimbatore, India.*
[c]*Northern Border University, College of Engineering, Mechanical Engineering Department, 91431, Arar Saudi Arabia.*

Received: November 13, 2023; Revised: March 05, 2024; Accepted: June 04, 2024

The combination of nickel (Ni) and titanium alloy (Ti) with silicon carbide (SiC) reinforcement offers promising avenues for research and applications due to their exceptional resistance to heat, oxidation, and corrosion properties. These studies investigate the influence of silicon carbide (SiC) on Ni-Ti matrix materials, focusing on Ni-Ti-SiC composites fabricated through the microwave sintering method. The microstructure analysis reveals uniform dispersion of Ni and Ti, indicating desirable properties. This study utilized the Taguchi methodology to optimize the wear rate of Ni-Ti-SiC composites by examining sliding distance, load, and sliding velocity as essential variables. The experimental findings showed a minimum wear rate of 0.014 mg/m under certain conditions and a maximum of 0.052 mg/m under other conditions. The optimal wear rate was determined using the signal-to-noise ratio (SN ratio) at a sliding distance of 1500 m, load of 20N, and sliding velocity of 1 m/s. Sliding distance was found to be the most significant factor affecting wear rate (55%), followed by load (32%) and sliding velocity (7.3%) according to the variance analysis. Scanning electron microscope (SEM) analysis showed increased wear grooves and a smoother surface in the specimen with the lower wear rate. Atomic force microscopy was used to analyze the worn surfaces, revealing detailed 3D image patterns. Surface parameters showed significant variations between surfaces with higher and lower wear rates. Surfaces with lower wear rates exhibited minimum average roughness (6.69 nm) and maximum peak-to-valley roughness (88.65 nm).

Keywords: *Nickel, titanium, silicon carbide, sintering, wear, Taugchi.*

1. Introduction

Titanium and Nickel alloys are pivotal in the automotive and aerospace industries, renowned for their robustness, chemical resistance, and biocompatibility[1,2]. The combination of Nickel and Titanium alloy with silicon carbide reinforcement in materials science presents a promising avenue for research and applications due to its exceptional resistance to heat, oxidation, and corrosion properties[3,4]. Reinforcing ceramics with SiC, B_4C, MgO, TiC, and ZnO enhances wear resistance and matrix material strength. SiC particles, widely embraced, reduce thermal expansion coefficients, enhancing material properties[5-7]. Powder sintering, a widely adopted manufacturing technique for these alloys, claims the capability to craft intricate shapes, deliver high specific strength, exert precise control over microstructure, minimize alloying element loss, ensure cost-effectiveness, conserve materials, and allow customization. These attributes make powder metallurgy and sintering composites attractive, offering outstanding mechanical, thermal, and electrical properties[8-10]. Powder metallurgy (PM) involves three main processes: powder production, compaction into green compact, and sintering. This process produces a near-net shape product with improved properties. Sintering involves heating a material below its melting point to promote bonding and densification. There are various methods, including Hot isostatic pressing (HIP)[11], Spark Plasma Sintering[12], microwave sintering[13], and Selective Laser Sintering[14], depending on the material and application. Conventional casting makes it difficult to establish a matrix-reinforcement particle size ratio. However, MMC synthesized by PM can achieve near-net shape samples and a matrix-filler size ratio close to one[15].Sliding wear tests on hybrid composites using the Hot Isostatic Pressing (HIP) technique showed a linear increase in volume loss over time. Balasundar et al.[16] investigated the wear behavior of Ti-0.8Ni–0.3Mo/TiB composites manufactured through microwave sintering. The addition of TiB enhanced the wear resistance and reduced the coefficient of friction. Farhadinia et al.[17] showed that increasing the amount of reinforcement decreased wear rates and friction coefficients. However, because of coarse Si particles, Spark Plasma Sintering resulted in micro-cracking and poor tribological performance[18]. Krakhmalev and Yadroitsev[19] have successfully created titanium carbides and silicate composites using selective laser melting of Ti-SiC powder mixtures, resulting in high hardness and abrasive wear resistance, improved laser penetration depth, and mass transport despite the high cost.The addition of 15wt% TiB in Ti-0.8Ni–0.3Mo improved the microhardness values from 220 to 260 HV[20]. Magnesium hybrid composites achieved enhanced wear resistance by incorporating 10% TiC and 7.5 wt. % MoS_2 particles[21,22]. Rajabi et al.[23] studied nano-

*e-mail: php1840@gmail.com

ZrO_2 particles in aluminum powder, resulting in a uniform reinforcement distribution and improved strength, with the optimal reinforcement, after compacting and sintering using microwave-assisted sintering.Microwave sintering allows for the customization of material porosity for various applications, such as filtration, catalysis, and tissue engineering. Studies using ammonium hydrogen carbonate revealed increased porosities and average pore sizes in porous Ni-Ti alloys, reduced hardness, compressive strength, elastic modulus, bending strength, and superelasticity[24]. Many researchers have used SiC as reinforcement in various matrix materials, improving hardness and reducing compressive strength. Wu et al.[25] reported superior Si-SiC 3D skeleton properties. Abdizadeh et al.[26] found that Al-SiC metal powder composites had increased hardness. Magnesium composites containing nano SiC particles were fabricated by Jingli Shang et al.[27]. who also improved the microstructure of the matrix to decrease age hardening. Gul Tosun and Mehmet Kurt[28] developed composite materials for Al and Mg using micro-sized SiC and Al2O3 particles, with the composite strengthened by 15% SiC having the highest porosity ratio at 17%. 316L stainless steel matrix was found to have improved micro-hardness and enhanced corrosion resistance by Wu et al.[29]. Incorporating SiC nanoparticles led to an increase in microhardness and a more complex phase structure, with more Ni3Ti phase and better martensitic stability[30].When compacts are heated in traditional furnaces, the microstructure becomes coarser and less uniform[31]. In order to reduce processing times and energy consumption, microwave heating can achieve homogeneous and rapid sintering by interacting directly with particulates[32]. This technique speeds up chemical reactions and shortens sintering times by a factor of 10[33]. In their research, Oke et al.[34] optimized the process parameters for Spark Plasma Sintering (SPS) to develop nano-structured duplex stainless steel reinforced with titanium nitride. The composites were thoroughly characterized using X-ray diffraction and scanning electron microscopy. The optimum properties were achieved in composites sintered at 1150°C for 15 minutes with a heating rate of 100°C per minute. Notably, the composites exhibited similar shrinkage behavior, with three distinctive peaks indicating a robust densification process[35]. In another study, process parameters for microwave sintering were optimized using the Taguchi approach. The resulting composites demonstrated an impressive tensile strength of 360 MPa when sintered at 1400°C, with a heating rate of 20°C per minute, for 80 minutes[36].

Existing literature provides valuable insights into the synthesis methods and microstructural characteristics of Ni-Ti-SiC composites. However, there is a research gap regarding the wear behavior of these composites, especially under varying conditions of load, sliding distance, and velocity.This study aims to fill the identified research gap by systematically investigating the wear behavior of Ni-Ti-SiC composites fabricated through microwave sintering. Comprehending the wear characteristics of Ni-Ti-SiC composites is essential for their successful use in applications like automotive and aerospace components. Addressing this research gap will help develop materials with enhanced wear resistance customized for particular uses. Taguchi based optimization technique was employed to predict the wearbeahviour of Ni-Ti-SiC composites during the dry sliding conditions.To gain insight into the microstructures of these composites, a range of analytical techniques, including X-ray diffraction, optical microscopy, scanning electron microscopy, and surface tests, are employed.

2. Materials and Methods

The material used in this study is nickel, titanium and silicon carbide particles. Nickel and titanium were used as matrix material, and reinforcement was silicon carbide. Silicon carbide is chosen for its high strength, thermal conductivity, and resistance to oxidation, temperature, and chemical influences. Initially, all three powders were ball milled using a ball milling machine with process parameters of rotational speed (250 rpm) and time duration (2 hrs). The powder was compacted using cold pressing process with compact pressure of 35 MPa at a temperature of 40°C. Followed by compact, microwave sintering was done with process parameter of temperature 1250°C and duration of 30 minutes. With the assistance of microwave heating, green samples were transformed entirely into sintered samples at a heating rate ranging from 20 to 30°C per minute. However, microwave heating rate was monitored by external infrared pyrometer. This process plays an essential role in developing components with excellent qualities. Figure 1a-f illustrates the complete fabrication process of powder-sintered specimen.

Initially, microhardness measurement was performed using computerized Vickers hardness measuring instrument. The specimen is prepared as per the ASTMG99 standard for conducting the dry wear test[22]. The wear behavior of sintered Ni-Ti-Sic composite specimens was evaluated through experimentation utilizing a pin-on-disc apparatus. The X-ray diffraction (XRD) technique was used to determine the phase composition of the sintered sample. Scanning Electron Microscopy (SEM) analysis was employed to investigate the worn-out surfaces under different load circumstances, thereby uncovering alterations in the microstructure, patterns of abrasion, and the extent of material degradation.

3. Experimental Design

A Design of Experiments (DoE) methodology notable for its reliability is the Taguchi technique. In this methodology, the various process factors are systematically recorded and examined in order to determine their effect on the overall process. Numerous studies have effectively employed this methodology to investigate the sliding wear characteristics of aluminum matrix composites. The tests conducted in this study were designed based on the typical orthogonal array. An orthogonal array with degrees of freedom higher than or equal to the total number of tested parameters is a requirement for Taguchi's approach. The estimation of wear rate of Ni-Ti-SiC composite depend upon following parameters such as load (N), sliding distance (m) and velocity (m/s). The criteria and their weights taken into account in this investigation are listed in Table 1. The reason for choice of L9 orthogonal array in the current research is to study the effect of wear process parameter in detail. Table 2 illustrates its nine rows and three columns.

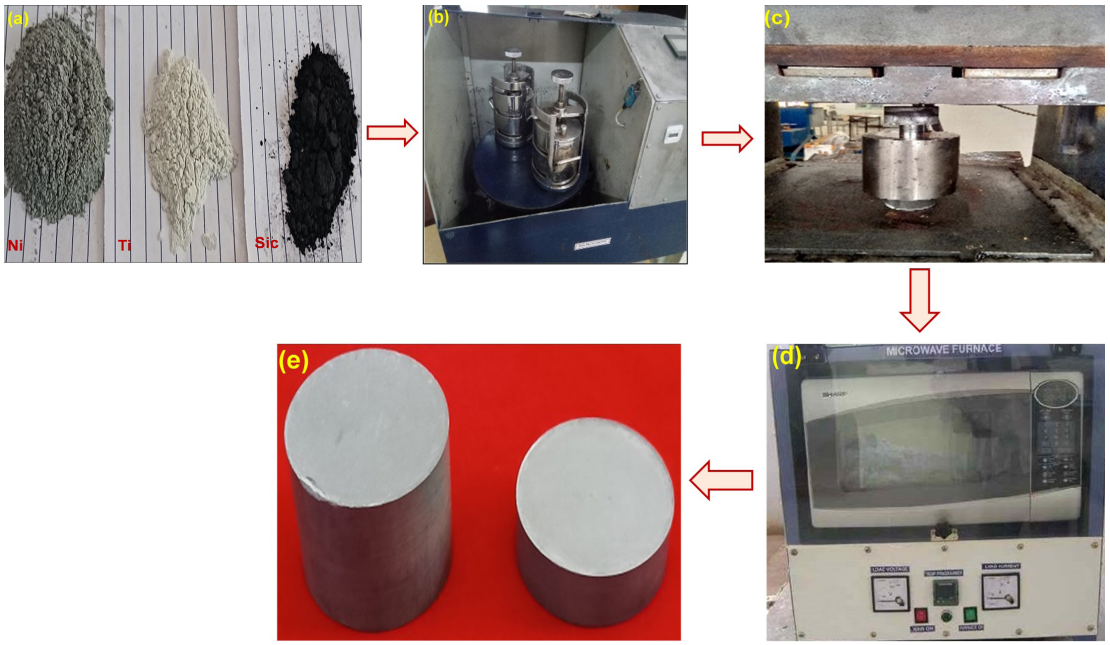

Figure 1. Fabrication process of Ni-Ti-SiC composite (a) Powders (b) Ball milling (c) Compacting (d) Sintering (e) Powder-sintered specimen.

Table 1. Wear process parameters and levels.

Parameters	Load (N)	Velocity (m/s)	Distance (m)
1	20	500	500
2	40	1000	1000
3	60	1500	15000

Table 2. L_9 orthogonal array.

Ex.No	Load	Distance	Velocity
	(N)	(m)	(m/s)
1	20	500	1
2	40	500	2
3	60	500	3
4	20	1000	2
5	40	1000	3
6	60	1000	1
7	20	1500	3
8	40	1500	1
9	60	1500	2

4. Results and Discussion

4.1. Microhardness& Microstructure

The hardness of the composite was measured as per ASTM E384[20] (load: 0.1 kg, dwell time: 15s). Microhardness value of the Ni-Ti-SiC composite was 312 HV. Figure 2 shows that the SEM images of Ni, Ti and SiC powders. Ni and Ti powders are spherical and droplet-like morphologies, whereas the morphology of SiC particles is ellipsoidal shape with sharp edges, tips and points. The SEM images of Ni-Ti-SiC composites after sintering are shown in Figure 3a. Ni adhering to Ti particles on the surface is noticed. SiC particles form microstructure clusters, varying in size and distribution, possibly due to the sintering process and initial characteristics. The uniform dispersion of Ni and Ti suggests that the composite may possess desirable properties due to the consistent distribution of these elements. To address SiC clustering, potential mitigation strategies, such as modifying the SiC particle size distribution[1].

Figure 3b shows the SEM and EDS results of Ni-Ti-SiC composite specimens. The chemical composition of composite was confirmed by EDS results, revealing a composition of 50% Ni, 48% Ti, and 2% SiC. Pore was seen as a result of the diffusion of Ti atoms into the Ni areas, which is occurred due to the difference in the mass transfer.

The high porosity between green grains of Ti and Ni powders, along with a larger intrinsic diffusion coefficient of nickel in titanium than that of titanium in nickel, results in vacancy formation in the inter diffusion zones of the sample. Additionally, the introduction of SiC further influences the diffusion process, impacting the composite's overall microstructure and mechanical properties. The density of the sample was assessed using the Archimedes method, and the porosity was calculated by a Formula 1[37].

$$P = \frac{m\ theoretical\ - m\ actual}{m\ theoretical} \times 100$$

$$m\ theoretical\ = \rho\ s\ \times v\ s$$

$$\rho\ s\ = \rho\grave{e}\ NiTi\ + \rho\grave{e}\ SiC$$

Where,
θ(NiTi) = Volume fraction of NiTi
θ(SiC) = Volume fraction of SiC

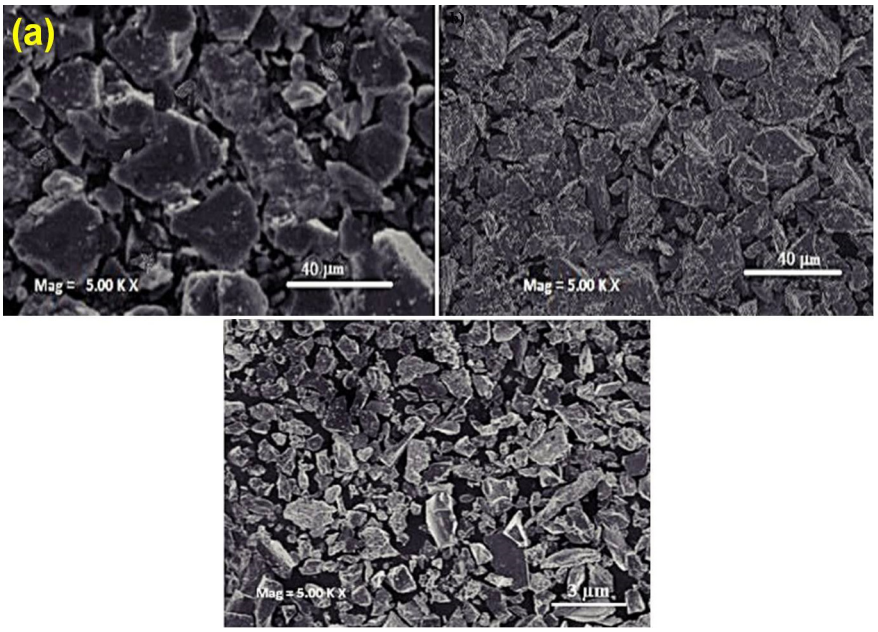

Figure 2. SEM images of powder a) Ni b) Ti c) SiC.

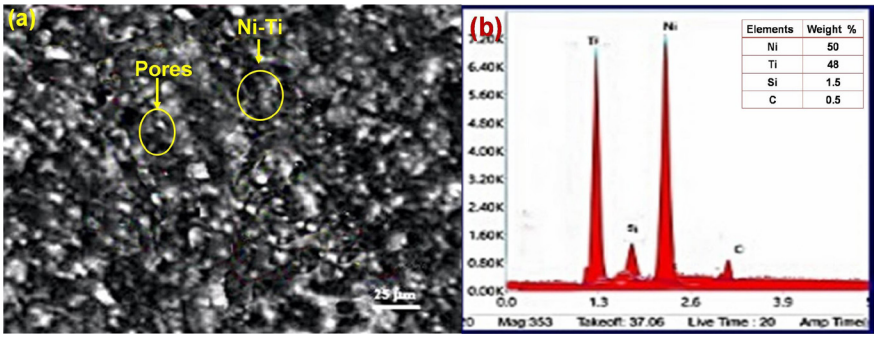

Figure 3. Ni-Ti-SiC composite (a) SEM (b) EDS.

$\rho(s) = 6.5\ cm^{-3} \times 0.98 + 3.21\ cm^{-3} \times 0.02$
$\rho(s) = 6.4342\ cm^{-3}$
$v(s) = 2.3565\ cm^{-3}$
m (theoretical) = 15.16 g
m (actual) = 14.02 g
Porosity percentage of Ni-Ti-SiC composite (P) =7.5%

The XRD analysis revealed specific crystallographic planes for titanium, silicon, carbon, and nickel, providing valuable insights into the structural properties of the synthesized material. Figure 4 depicts the XRD results of Ni-Ti-SiC composites.

The presence of (110) Ti, (004) Si, (202) C, and (113) Ni planes aligns with the crystal structures documented in the reference PDF card 04-007-3753. The observed XRD peaks indicate the successful synthesis of the Ni-Ti-SiC composite, confirming the presence of relevant crystal phases from the Ni and Ti components and the SiC additive. The sintering process was stable, without unexpected chemical reactions or phase transformations.

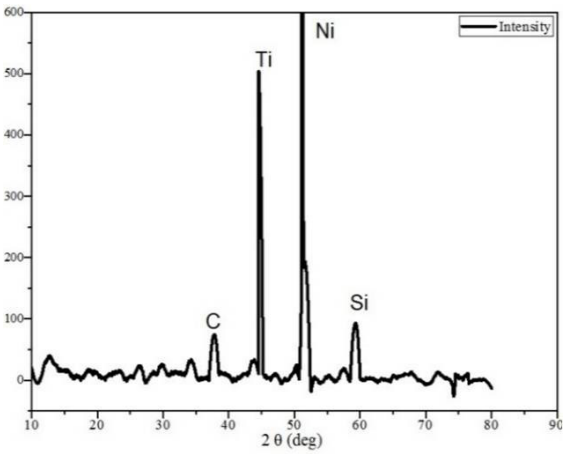

Figure 4. XRD peaks of Ni-Ti-SiC composite.

4.2. Wear analysis

The Taguchi methodology is a highly effective approach used for identifying the optimal wear rate of Ni-Ti-SiC composites.The wear rate was assessed by considering different input limitations associated with the wear variables. The wear rate's sliding distance, load, and velocity are necessary. Table 3 illustrates the experimental findings pertaining to the wear rate.

The experimental results yielded a maximum wear rate of 0.052 mg/m under a sliding distance of 500 m, a load of 40N, and a sliding velocity of 3 m/s. A minimum wear rate of 0.014 mg/m was achieved under the experimental conditions of a sliding distance of 1500m, a load of 20N, and a sliding velocity of 3 m/s. The addition of reinforcement material in Ni-Ti reduces the loss of material due to wear. Thus, the wear resistance of the Ni-Ti composite increases with the addition of SiC. The other possible factor for enhancing wear properties is a reduction in the effective contact area between the composite pin and counter disc due to the addition of reinforcement particles. At a more considerable sliding distance, the contact time between the pin and the rotating hard steel disc increases, resulting in increased heatgeneration[36]. The high heat generation softens Ni-Ti matrix material around SiC particles worn out, making harder ceramic particles protrude out of the pin surface. Thus, the load applied on the composite pin is partially taken by SiC particles, reducing the contact area and wear loss. The addition of SiC ceramic particles in the Ni-Ti matrix reduces the ductile property of the matrix material, which reduces the adhesive wear of the material. It was the reason for the drastic variation of values between sliding distances (1000 and 1500 m).The responses, including the SN ratio and mean for the wear rate, were determined based on the smaller-the-better criterion and are shown in Table 4. The best level of the control factors is essential for the performance and SN ratio. The SN ratio affects the process's unpredictability and intended ideal characteristics. It will help analyze the process's mean and standard deviation.

Table 3. Experimental results.

Ex.No	Load	Sliding Distance	Sliding Velocity	Wear rate
	(N)	(m)	(m/s)	(mg/m)
1	20	500	1	0.023
2	40	500	2	0.035
3	60	500	3	0.052
4	20	1000	2	0.026
5	40	1000	3	0.032
6	60	1000	1	0.039
7	20	1500	3	0.014
8	40	1500	1	0.018
9	60	1500	2	0.019

An orthogonal array experimental design can investigate the effect of several different variables on the concert attributes in a small range of experiments. The selection of the optimal wear rate was determined by evaluating the effect of the signal-to-noise ratio (SN ratio), as depicted in Figure 5.

The optimal wear rate was arrived at a sliding distance (1500 m), load (20N) and sliding velocity (1 m/s). The effect of various input limitation on the response factor was estimated using variance analysis. As shown in Table 5, the sliding distance was the most significant contribution factor (55%) to the wear rate of the Ni-Ti-SiC composite. The second most influential factor was the load (32%), followed by the sliding velocity (7.3%). The primary effect of sliding distance on wear resistance compared to the load in the wear test of the Ni-Ti-SiC composite was mainly attributed to the combined impact of wear over a longer distance. An increase in sliding distance has a more significant advantage for abrasive particles, frictional forces and other wear mechanisms to act on the composite material, leading to progressive material loss and wear rates[21]. The load certainly influences the contact pressure and can lead to wear. However, its effect might be more localized than the cumulative effect of sliding distance.

$$\text{Wear rate (mg/m)} = 0.02867 + 0.00800 \times A - 500 + 0.00367 \times A - 1000 - 0.01167\times A - 1500 - 0.00767 \times B - 20 - 0.00033 \times B - 40 + 0.00800 \times B - 60 - 0.00200 \times C - 1 - 0.00200 \times C - 2 + 0.00400 \times C - 3 \quad (1)$$

The wear rate regression equation is shown in Equation 1. Where A, B, and C are the input constraints for the wear-test factors. This was used to predict the wear rate of the Ni-Ti-SiC composite. The model summary is shown in Table 6.

4.3. Contour plot analysis

A contour plot was utilized to investigate the relationship between the input and output variables and their effects. The effects of the sliding distance vs load, sliding velocity vs load and sliding distance vs sliding velocity on the wear rate are shown in Figure 6a-c.

Table 4. Responses of SN ratio and Means for wear rate.

Stages	SN ratio			Means		
	Load	Sliding Distance	Sliding velocity	Load	Sliding Distance	Sliding velocity
1	29.19	33.85	31.95	0.03667	0.02100	0.02667
2	29.93	31.30	31.75	0.03233	0.02833	0.02667
3	35.47	29.43	30.88	0.01700	0.03667	0.03267
Delta	6.28	4.42	1.06	0.01967	0.01567	0.00600
Grade	1	2	3	1	2	3

Table 5. ANOVA of wear rate.

Source	DF	Adj.SS	Adj.MS	F	P	%
Sliding distance	2	0.000641	0.000320	7.75	0.114	55.06
Load	2	0.000369	0.000184	4.46	0.183	31.70
Sliding velocity	2	0.000083	0.000041	0.87	0.534	07.31
Error	2	0.000072	0.000036	----	----	05.93
Total	8	0.001164	----	----	----	100

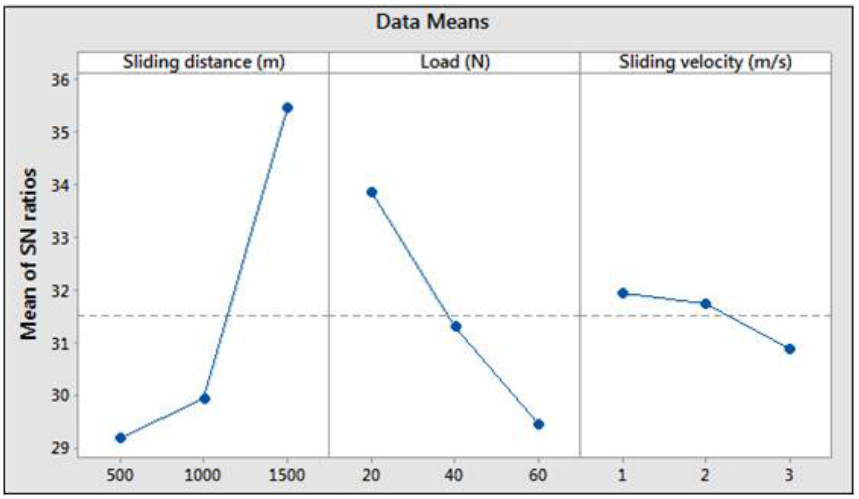

Figure 5. SN ratio graph.

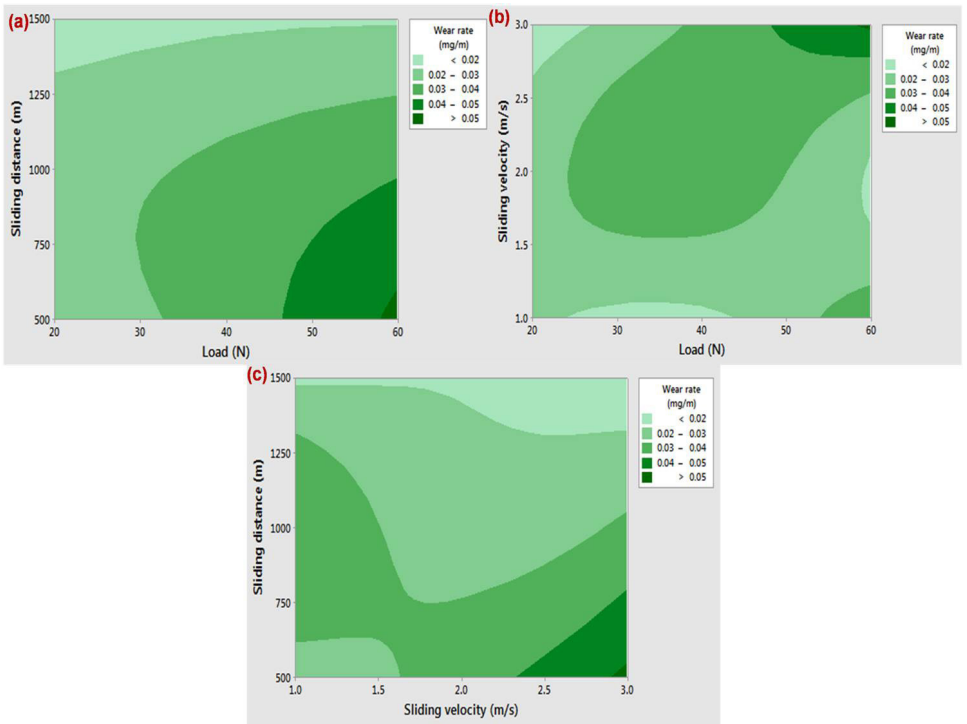

Figure 6. (a)Sliding distance and load on the wear rate(b) Sliding velocity and load on the wear rate(c)Sliding distance and sliding velocity on the wear rate.

Table 6. Model summary.

S	R-sq	R-sq(adj)	R-sq(pred)
0.0064291	92.90%	71.59%	0.00%

At a sliding distance of 1500 meters and an applied load ranging from 20 to 30 N, a low wear rate of less than 0.02 mg/m was achieved. However, when the sliding distance was reduced to 500-750 meters, and the load increased to 50-60 N, the wear rate increased to more than 0.05 mg/m. Similarly, with a sliding velocity of 3 m/s and a load of 25-40 N, a low wear rate of less than 0.02 mg/m was observed. Conversely, as the load increased from 50 to 60 N, along with the highest sliding velocity, the wear rate increased to more than 0.05 mg/m. Finally, at a sliding distance of 1500 meters and a sliding velocity of 2-3 m/s, a low wear rate of less than 0.02 mg/m was achieved. However, when the sliding distance was reduced to 500-750 m, and the sliding velocity was maintained at 2.5-3 m/s, the wear rate increased to more than 0.05 mg/m. The effect of individual factors on wear rate was analyzed using a Pareto chart, as shown in Figure 7a-c.

Figure 7a illustrates the impact of load on wear rate. According to the graph, under a load of 20N, wear rates of 0.014, 0.026, and 0.023 mg/m were achieved. At a load of 40N, wear rates of 0.018, 0.032, and 0.035 mg/m were

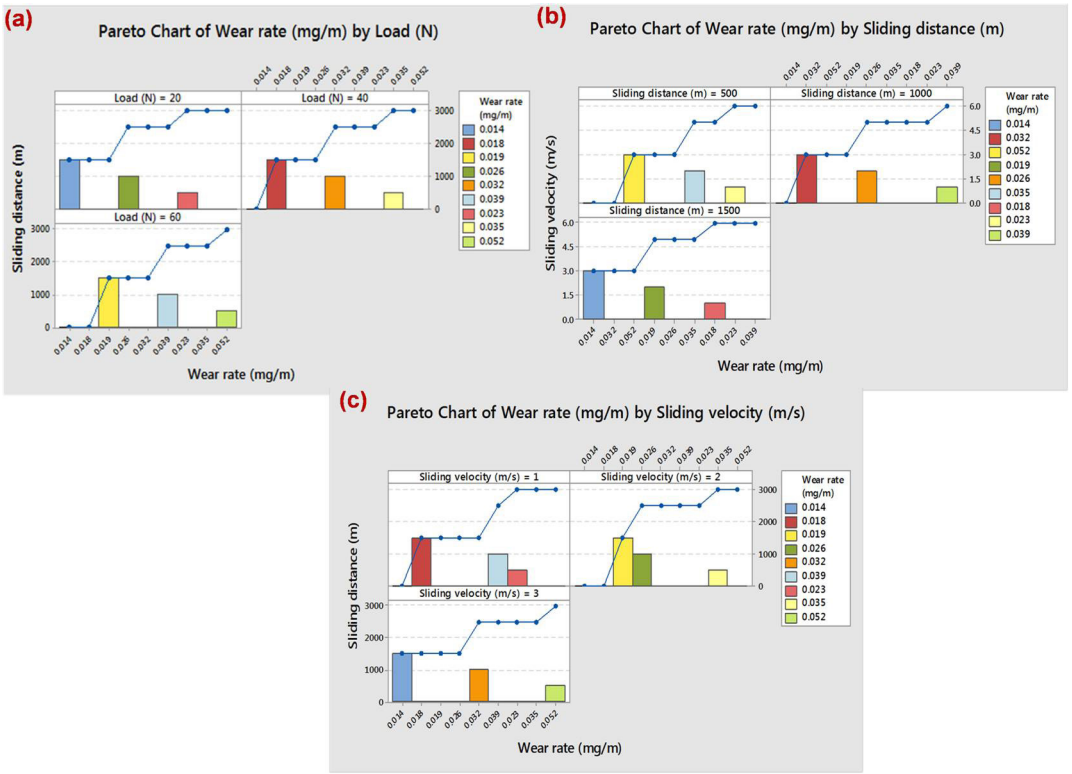

Figure 7. (a) Wear rate by load(b) Wear rate by sliding distance (c)Wear rate by sliding distance.

attained. At a load of 40N, wear rates of 0.019, 0.039, and 0.052 mg/m were recorded. Therefore, for a load of 20N, a low wear rate was achieved. The effect of the sliding distance on the wear rate is shown in Figure 7b. The chart shows wear rates of 0.052, 0.035, and 0.023 mg/m at a sliding distance of 500 m. At a sliding distance of 1000m, wear rates of 0.032, 0.026, and 0.039 mg/m were discovered. At a 1500m sliding distance, wear rates of 0.014, 0.019, and 0.026 mg/m were measured. Consequently, a low wear rate is reached at a 1500 m sliding distance. Figure 7c depicts the wear rate's sliding velocity. At a sliding speed of 1 m/s, wear rates of 0.018, 0.039, and 0.023 mg/m were determined from the chart. At a sliding speed of 2 m/s, wear rates of 0.019, 0.026, and 0.035 mg/m were recorded. At a 1500m sliding distance, wear rates of 0.014, 0.032, and 0.052 mg/m were measured. As a result, a low wear rate is achieved at 2 m/s sliding velocity.

4.4. Worn surface

Figure 8a-d shows the SEM images of the higher (0.052 mg/m), intermediate (0.035 mg/m), lower (0.023 mg/m) and shallow (0.014 mg/m) worn-out specimens of Ni-Ti-SiC composites, respectively. The sliding distances of all the specimens are shown as inclined lines. More significant wear debris was noticed on the higher worn surfaces (Figure 8a) as a result of the intense abrasive action between the pin and work piece.

The sliding motion and the pin also caused delamination, which tends to peel off the surface and leave behind flake particles.The maximum force on the tool pin was one of the reasons for the delamination of the intermediate surface (Figure 8b). Delamination wear occurs by significant plastic deformation of the surface layer, resulting in the formation of wear debris. Delamination is thought to be caused by a difference in the elastic properties of superelastic Ni-Ti-Sic throughout the sample cross-section, resulting in increased delamination[38].The formation of delamination along with wear debris due to the abrasive action of the contact surface. The micro-ploughing action was formed in between the contact surfaces was the reason for occurrence of pullout material in the higher and intermediate wear surfaces. A similar phenomenon was noticed in the Ni-Ti composites[39]. The surface featured longitudinally oriented grooves along the sliding direction. The grooves were formed by the counter-face's ploughing action and loose wear debris caused by third-party abrasion. The ridges surrounding the grooves deform and fracture, leading to the creation of wear debris. Due to the uneven particle bonding and the strong force acting on the pin during the wear test, pull-out material dispersed across the surface was evident, as noticed in the very low-wear surfaces. A strong force produces a worn-out surface that causes a high frictional force between the tool pin and the work piece. Some layers from the surface were agglomerated and merged during the wear test in a process known as material binding, also known as the material transfer layer. The wear rate exhibited a progressive increase as the loading conditions increased. Due to this phenomenon, wear debris can be identified in Figures 8c and 8d at some locations. The presence of wear debris in the significantly lower wear rate specimens (0.014 mg/m) was less than in all other conditions. The lower wear debris in the specimens at higher sliding distance confirms that composites manufactured

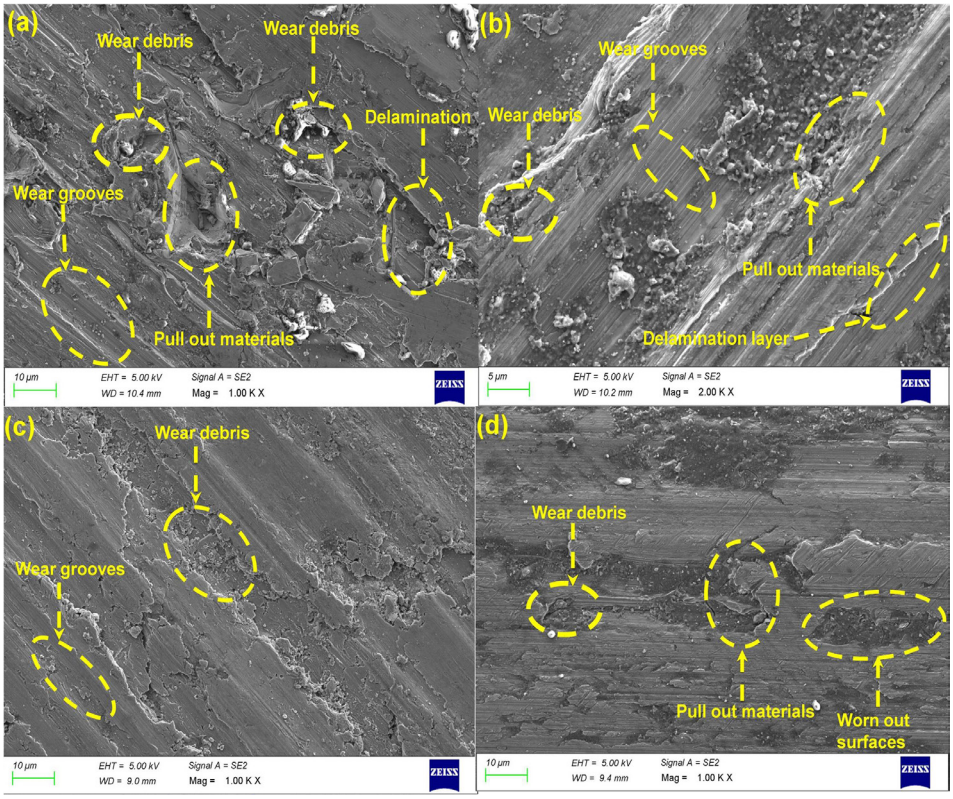

Figure 8. SEM images (a) Higher worn surface (0.052 mg/m) (b) Intermediate worn surface (0.035 mg/m) (c) Lower worn surface (0.023 mg/m) (d) Shallow worn surface (0.014 mg/m).

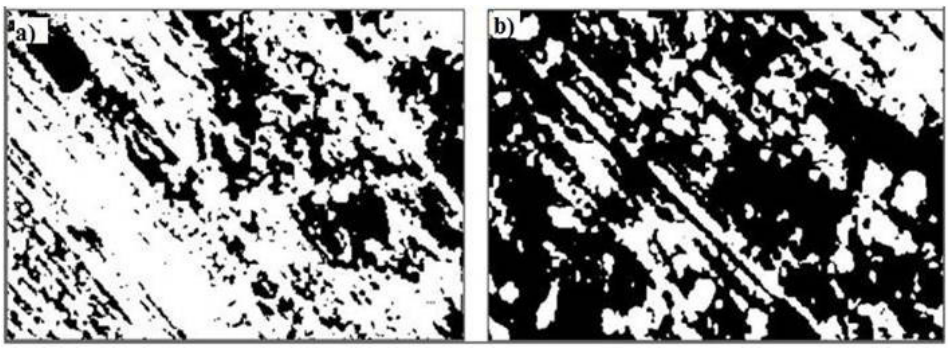

Figure 9. Threshold image of composite at (a) higher wear rate (b) lower wear rate.

with dense microstructure and controlled porosity. The large sliding distance soften the Ni-Ti matrix material around SiC particles worn out, making harder ceramic particles protrude out of the composites results minimum wear debris compare to other conditions. The presence of SiC layer reduces the detachment and wears debris formation. The formation wearsdebris in all the condition owing to adhesive wear. Similar type wear failure was noticed for Ni-Ti composites[39].

The threshold image of the SEM picture of the worn-out specimen taken at the maximum and minimum wear rate, respectively, is shown in Figures 9a and b. Image segmentation is one of the most critical tasks in SEM images for extracting grain boundaries from the background. Generally, this is achieved by converting any image into a binary image. It consists of only black-and-white images. Image segmentation mainly focused on identifying black spots quickly from the binary image. It was essential to analyze how the particles distorted during the wear test in this test. Figure 9a and b show the clustered particles spotted over the surface. The higher wear rate specimen noticed more wear grooves than the lower wear rate. Moreover, the SEM image showed a smooth surface without evidence of many materials in the inferior wear rate specimen.

4.5 Atomic force microscopic analysis of worn surfaces

The atomic force microscope study helped analyze the wear parameters and visualize the 3D image pattern of the SEM image. In Figure 10a, a black spot is noted, which defines the wear debris during the wear test. In some places,

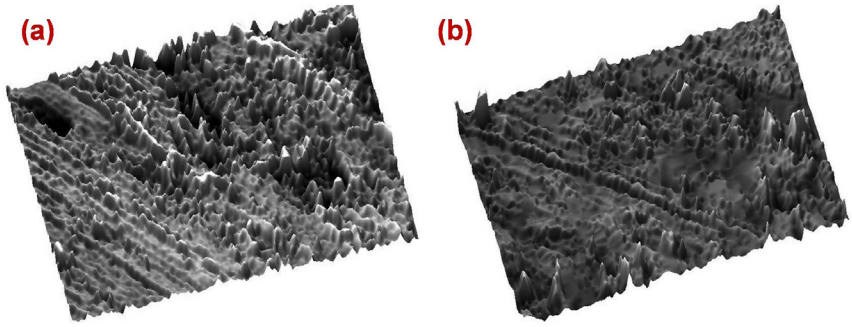

Figure 10. AFM image (a) Higher worn surface (b) Lower worn surface.

Table 7. Surface parameters.

Sl.no	Surface parameters	Higher wear rate surface	Lower wear rate surface
1	Roughness average (Ra)	22.75 nm	6.69 nm
2	Root mean square roughness(Rq)	32.27 nm	10.05 nm
3	Maximum height of the roughness (Rt)	245.3 nm	97.85 nm
4	Maximum roughness valley depth (Rv)	86.49 nm	51.95 nm
5	Average maximum height of the roughness(Rtm)	167 nm	56.24 nm
6	Maximum peak to valley roughness (Rmax)	245.3 nm	88.65 nm
7	Skewness (Rsk)	0.1419	-0.2819
8	Kurtosis (Rku)	5.632	7.617

the profile had a higher number of peaks. It is indicated that the sliding method also represents the worn-out surface-like cavity profile in the image (Figure 10b). The peeled-off material was identified with a greater number of cavities present over the surface.

Table 7 represents the surface parameter values of the worn-out the specimen at the higher and lower worn surface. The table showed minimal average roughness value in the lower worn surface. The value was found to be 6.69 nm. The root-mean-square values for the two specimens were normal. The maximum height of the roughness value was found as 245.3 nm in the higher wear rate specimen, indicating that the bunch of material was bonded together during the wear test. The peak-to-valley roughness value was also the maximum for the higher-wear specimen. The surface profile mainly depends on essential factors such as skewness and kurtosis.

5. Conclusion

This study investigates the wear behavior of Ni-Ti-SiC composites fabricated through the microwave sintering method. The research systematically examines the effects of SiC particle concentration and sintering duration on wear resistance, employing dry sliding wear tests.

- The results highlight the significance of the chosen fabrication process, showcasing uniform dispersion of Ni and Ti, which is indicative of desirable material properties. X-ray diffraction analysis confirms the successful synthesis of the Ni-Ti-SiC composite, affirming the presence of relevant crystal phases from Ni, Ti, and SiC components.
- The wear analysis, conducted under varying conditions of load, sliding distance, and velocity, demonstrates the intricate interplay of these parameters on wear rate. The Taguchi optimization technique identifies optimal wear rates, with sliding distance identified as the most influential factor. The contour plot analysis further illustrates the complex relationship between input and output variables, providing valuable insights for optimizing wear behavior.
- SEM images of worn surfaces offer visual confirmation of wear behavior, showcasing wear debris and material binding. Atomic force microscopic analysis complements these findings, offering a detailed 3D image pattern of the worn surfaces.
- In conclusion, this study not only advances our understanding of the wear behavior of Ni-Ti-SiC composites but also underscores the effectiveness of microwave sintering as a fabrication method. This research paves the way for further exploration and development of advanced materials with enhanced wear resistance properties.

6. References

1. SivakumarG, AnanthiV, RamanathanS. Production and mechanical properties of nanoSiC particle reinforced Ti–6Al–4V matrix composite.TNonferr Metal Soc. 2017;27:82-90.
2. BolzoniL, Ruiz-NavasEM, GordoE. Influence of sintering parameters on the properties of powder metallurgy Ti–3Al–2.5Valloy.Mater Charact. 2013;84:48-57.
3. ErdemirF, CanakciA, VarolT, OzkayaS. Corrosion and wear behavior of functionally graded Al2024/SiC composites produced by hot pressing and consolidation.J Alloys Compd. 2015;644:589-96.
4. IzadiH, NoltingA, MunroC. Friction stir processing of Al/SiC composites fabricated by powder metallurgy.Prog Mater Sci. 2013;213:1900-7.
5. SahinY. Tribological behaviour of metal matrix and its composite. Mater Des. 2007;28:1348-52.
6. SlipenyukA, KuprinV, MilmanYU, SpowartJE, MiracleDB. The effect of matrix to reinforcement particle size ratio(PSR) on the microstructure and mechanical properties of a P/M processed AlCuMn/SiCp MMC.Mater Sci Eng A. 2004;381:165-70.
7. KumaiS, HuJ, HigoY, NunomuraS. Effects of dendrite cellsize and particle distribution on the near-threshold fatigue crackgrowthbehaviour of cast Al-SiCp composites.Acta Mater. 1996;44:2249-57.
8. CavdarU, AtikE, AkgulMB. Magnetic-thermal analysis and rapid consolidation of Fe-3 wt% cu powder metal compacts sintered by medium-frequency induction-heated system.Powder Metall Met Ceramics. 2014;53:191-8.

9. GeniM, KikuchiM. Damage analysis of aluminum matrixcomposite considering non-uniform distribution of SiCparticles.Acta Mater. 1998;46:3125-33.
10. BoselliJ, PitcherPD, GregsonPJ, SinclairI. Numericalmodelling of particle distribution effects on fatigue in Al–SiCpcomposites. Mater Sci Eng A. 2001;300:113-24.
11. GreinerC, OppenheimerSM, DunandDC. High strength, low stiffness, porous NiTi with superelastic properties.Acta Biomater. 2005;1(6):705-16.
12. ZhaoY, TayaM, KangY, KawasakiA. Compression behavior of porous NiTi shape memory alloy.Acta Mater. 2005;53(2):337-43.
13. EsinA, MahmutyazıcıoğluN, AltıntaşS. Drying and sintering of ceramic based parts using microwave heating.Key Eng Mater. 2004;264:731-4.
14. SimchiA. Direct laser sintering of metal powders: mechanism, kinetics and microstructural features.Mater Sci Eng A. 2006;428(1-2):148-58.
15. SlipenyukA, KuprinV, MilmanY, GoncharukV, EckertJ. Properties of P/M processed particle reinforced metal matrix composites specified by reinforcement concentration and matrix-to-reinforcement particle size ratio.Acta Mater. 2006;54(1):157-66.
16. BalasundarP, SenthilS, NarayanasamyP, RamkumarT. Microstructure and tribological properties of microwave-sintered Ti0. 8Ni–0.3 Mo/TiB composites.Ceram Int. 2023;49(4):6055-62.
17. FarhadiniaF, SedghiA. Wear behaviour of Al/(Al2O3+ ZrB2+ TiB2) hybrid composites fabricated by hot pressing.Int J Mater Res. 2021;106(2):160-5.
18. TkachenkoS, CizekJ, MušálekR, DvořákK, SpotzZ, MontufarEB, et al. Metal matrix to ceramic matrix transition via feedstock processing of SPS titanium composites alloyed with high silicone content.J Alloys Compd. 2018;764:776-88.
19. KrakhmalevP, YadroitsevI. Microstructure and properties of intermetallic composite coatings fabricated by selective laser melting of Ti–SiC powder mixtures.Intermetallics. 2014;46:147-55.
20. BalasundarP, SenthilS, NarayanasamyP, RamkumarT. Mechanical, thermal, electrical, and corrosion properties of microwave-sintered Ti-0.8 Ni-0.3 Mo/TiB composites.Phys Scr. 2023;98(6):065954.
21. SelvakumarN, NarayanasamyP. Optimization and effect of weight fraction of MoS2 on the tribological behavior of Mg-TiC-MoS2 hybrid composites.Tribol Trans. 2016;59(4):733-47.
22. NarayanasamyP, SelvakumarN. Effect of hybridizing and optimization of TiC on the tribological behavior of Mg–MoS2 composites.J Tribol. 2017;139(5):051301.
23. RajabiM, KhodaiMM, AskariN. Microwave-assisted sintering of Al–ZrO 2 nano-composites.J Mater Sci Mater Electron. 2014;25:4577-84.
24. XuJL, BaoLZ, LiuAH, JinXJ, TongYX, LuoJM, et al. Microstructure, mechanical properties and superelasticity of biomedical porous NiTi alloy prepared by microwave sintering. Mater Sci Eng C. 2015;46:387-93.
25. WuC, GaoT, LiuX. In-situ SiCreinforced Si-SiC 3D skeletons in SiC/Al-Si composites.J Alloys Compd. 2019;810:151730.
26. HassaniA, BagherpourE, QodsF. Influence a of pores on workability of porous Al/SiC composites fabricate through powder metallurgy–mechanical alloying.J Alloys Compd. 2014;591:132-42.
27. ShangJ, KeL, LiuF, FeiyueLV, XingL. Aging behavior of nanoSiC particles reinforced AZ91D composite fabricated via friction stir processing.J Alloys Compd. 2019;797:1240-8.
28. TosunG, KurtM. The porosity, microstructure, and hardness of Al-mg composites reinforced with micro particle SiC/Al_2O_3 produced using powder metallurgy.Compos, Part B Eng. 2019;174:106965.
29. WuCL, ZhangS, ZhangCH, ZhangJB, LiuY, ChenJ. Effects of SiC content on phase evolution and corrosion behaviorofSiC-reinforced 316L stainless steel matrix composites by laser melting deposition.Opt Laser Technol. 2019;115:134-9.
30. JiaC, AkbarpourMR, GharamalekiMA, EbadzadehT, KimHS. Synthesis and characterization of novel NiTi–Ni3Ti/SiC nanocomposites prepared by mechanical alloying and microwave-assisted sintering process.Ceram Int. 2023;49(14):23358-66.
31. PadmavathiC, UpadhyayaA, AgrawalD. Effect of microwave and conventional heating on sintering behavior and properties of Al–Mg–Si–Cu alloy.Mater Chem Phys. 2011;130(1-2):449-57.
32. BaghurstDR, ChippindaleAM, MingosDMP. Microwave syntheses for superconducting ceramics.Nature. 1988;332(6162):311-311.
33. ThakurSK, KongTS, GuptaM. Microwave synthesis and characterization of metastable (Al/Ti) and hybrid (Al/Ti+ SiC) composites.Mater Sci Eng A. 2007;452:61-9.
34. OkeSR, IgeOO, FalodunOE, ObadeleBA, ShongweMB, OlubambiPA. Optimization of process parameters for spark plasma sintering of nano structured SAF 2205 composite.J Mater Res Technol. 2018;7(2):126-34.
35. ThirumalvalavanS, SenthilkumarN, PerumalG, AnanthaMR, Padmanaban. Ameliorating the wear defiance of HVOF thermal spray silicon carbide coated Ti-6Al-4V alloy using PCA-GRA technique.Silicon. 2022;14:3101-17. http://doi.org/10.1007/s12633-022-01706-7.
36. ThirumalvalavanS, SenthilkumarN. Experimental Investigation and Optimization of HVOF spray parameters on wear resistance behaviour of Ti-6Al-4V alloy.Dokl Bulg Akad Nauk. 2019;72(5):665-74. http://doi.org/10.7546/CRABS.2019.05.15.
37. WangJ, HuK. Phase transformation of NiTi alloys during vacuum sintering.IOP Conf Series Mater Sci Eng. 2017;204(1):012023.
38. NeupaneR, FarhatZ. Wear mechanisms of nitinol under reciprocating sliding contact.Wear. 2014;315(1-2):25-30.
39. FarviziM, EbadzadehT, VaeziMR, YoonEY, KimY-J, KangJY, et al. Effect of starting materials on the wear performance of NiTi-based composites.Wear. 2015;334:35-43.